

# Extra-wide deposition in extrusion additive manufacturing: A new convention for improved interlayer mechanical performance

James Allum, Amirpasha Moetazedian<sup>1</sup>, Andy Gleadall\*, Niall Mitchell, Theodoros Marinopoulos, Isaac McAdam, Simin Li, Vadim V. Silberschmidt

Wolfson School of Mechanical, Electrical and Manufacturing Engineering, Loughborough University, Loughborough LE11 3TU, UK

## ARTICLE INFO

### Keywords:

Extra-wide deposition  
Mechanical properties  
DfAM  
Contact area  
Interlayer bond

## ABSTRACT

Recent studies have contested long-standing assumptions that mechanical anisotropy is caused by weak interlayer bonding and demonstrated that microscale geometry (the groove between extruded filaments) is the major cause of anisotropy in extrusion additive manufacturing (AM). Inspired by those findings, this study investigates the potential for a new convention for print-path design to improve mechanical properties by setting extrusion width to be at least 250 % of nozzle diameter. The new convention enabled an almost 50 % improvement in mechanical performance, which was supported by finite element analysis data, whilst simultaneously reducing the printing time by 67 %. Whereas a typical extrusion AM part uses several side-by-side extrusions, here, three 0.4-mm-wide extrusions are replaced with a single extra-wide 1.2-mm extrusion; two 0.6-mm-wide extrusions are also studied. The contact area between layers of the extra-wide extrusion was 90 % as opposed to 63 % for the conventional approach. The improved contact area led to a 40–48 % enhancement of strength, strain-at-fracture and toughness. This study presents a compelling case for a methodological shift to extra-wide extruded-filament deposition and explains the underlying cause of anisotropic strength observed in previous studies. Two case studies demonstrate practical applicability for a print run of 1000 nylon visors and lower-limb polylactide prosthetic sockets, for which extra-wide filaments more than doubled load-bearing capabilities. Polylactide material was used for most of the study; potential for translation to other materials is discussed.

## 1. Introduction

Material extrusion additive manufacturing (MEAM) has seen major development recently with particular research investment in high-value industries such as medical devices [1–4] and aerospace technologies [5, 6]. MEAM offers numerous advantages over traditional manufacturing, including increased design freedom [7,8] and the capability to achieve more complex geometries [9,10]. MEAM operates by extrusion of a polymer filament through a heated nozzle, depositing it onto a print platform below. Simultaneously, through X and Y movements of the nozzle, a geometry is sequentially dispensed in microscale layers. At the completion of each layer, the nozzle moves along the Z axis and subsequently deposits the next layer; this process is repeated to build the part layer-by-layer. The geometry of the part is governed by the toolpath; it is a physical embodiment of the toolpath defined as GCode.

It is widely known that interlayer weakness of MEAM-produced parts

is a significant obstacle limiting the application of MEAM in the manufacture of mechanical parts. Previous studies have demonstrated that mechanical properties are influenced by geometrical parameters, including layer height (LH) and extruded-filament width (EFW), and by thermal parameters, including extrusion temperature and speed. However, numerous contradictions were presented. For example, some works reported that lower speeds improved the mechanical performance [11–13], whilst others demonstrated the opposite trend [14,15]. Similarly, higher extrusion temperatures were shown to be mechanically beneficial in some studies [16–19], but did not have a significant effect in others [20,21].

These contradictions arose predominantly as a result of complex methodologies and significant variability in specimen-toolpath-generation approaches, in addition to the use of test methods not optimised for characterisation of MEAM parts. While it was previously proposed that incomplete interlayer bonding was the predominant cause

\* Corresponding author.

E-mail addresses: [j.allum@amrc.co.uk](mailto:j.allum@amrc.co.uk) (J. Allum), [A.Gleadall@lboro.ac.uk](mailto:A.Gleadall@lboro.ac.uk) (A. Gleadall).

<sup>1</sup> co-first author

of anisotropy [12,15,22–28], it has recently been proven that the interlayer bond can readily achieve bulk-material properties [29–33] and that geometrical narrowing and stress concentration caused by interlayer grooves and voids result in reduced interlayer mechanical performance. Studies [31,34] identified that mechanical performance could be improved by increasing the EFW in specimens formed by individual stacked filaments, but the implementation of these methods on parts built with multiple extruded filaments or with unconventionally large EFWs has not yet been investigated. Additionally, a correlation between increased neck growth and strength has been demonstrated computationally [35].

This study is the first study to consider extra-wide extruded filament widths (250% nozzle diameter) and the number of extruded filaments (single, double and triple) on interlayer mechanical performance and anisotropy of MEAM-produced specimens using both experimental and computational studies. All tensile-testing specimens here have the same overall outer width (1.2 mm) and polylactide material (PLA) but differ in their structure in terms of how many extruded filaments are used. The geometry from microscopy together with material properties from the literature are used for finite element analysis (FEA). This study aims to investigate the mechanical and geometrical implications of utilising an unconventional extra-wide EFW (1.2 mm for a 0.4 mm nozzle) to elucidate its potential mechanical benefits compared to conventional multifilament walls (with EFW of 0.4 mm and 0.6 mm) and inform improved conventions for design for additive manufacturing (DfAM). This is achieved by using three different specimen types with single (1.2 mm EFW), double ( $2 \times 0.6$  mm EFW) and triple ( $3 \times 0.4$  mm) walls to provide the same comparable overall specimen widths. The findings of this study are highly applicable for the development of perimeter and infill structures for ‘vase’-like printing strategies in MEAM. Analysis of different extruded-filament geometry combinations provides a new understanding and significant evidence to support new methodologies

for improved mechanical performance in the Z direction.

## 2. Materials and methods

### 2.1. Materials

Natural PLA filament (100% virgin PLA 3DXTECH® branded NatureWorks® polylactide 4043D, Sigma Aldrich) with a density of  $1.25 \text{ g.cm}^{-3}$  was as used to manufacture specimens. Bulk mechanical properties of the material were 62.8 MPa, 2.65 GPa and 0.0507 for ultimate tensile strength, tensile modulus and strain at break, respectively [36]. PLA is a widely used 3D printing material and is particularly important for biomedical applications [37]. No lot number is available for the material, but multiple batches have been used in previous studies by the authors, including 1.75-mm and 2.85-mm variants, and similar properties were always found.

### 2.2. Additive manufacturing process

All specimens for this study were manufactured using PLA filament with a Reality Ender 3 Pro 3D-printing system. Three toolpath designs were developed for two filament orientations (Fig. 1) using FullControl GCode Designer [38] for direct control of geometry and deposition sequences [39]. Dogbone geometries with controlled incremental variation of extrusion width were manufactured to enable tensile testing. The design was adapted from the microtensile specimen, ASTM D1708 [40]. Specimens were produced in both Z direction, with extruded filaments oriented normal to the direction of loading (transverse), and in filament (F) direction with extruded filaments oriented in the direction of loading (longitudinally).

Specimens were printed with an overall outer width of 1.2 mm, achieved in three different formats for both F and Z orientations (Fig. 1

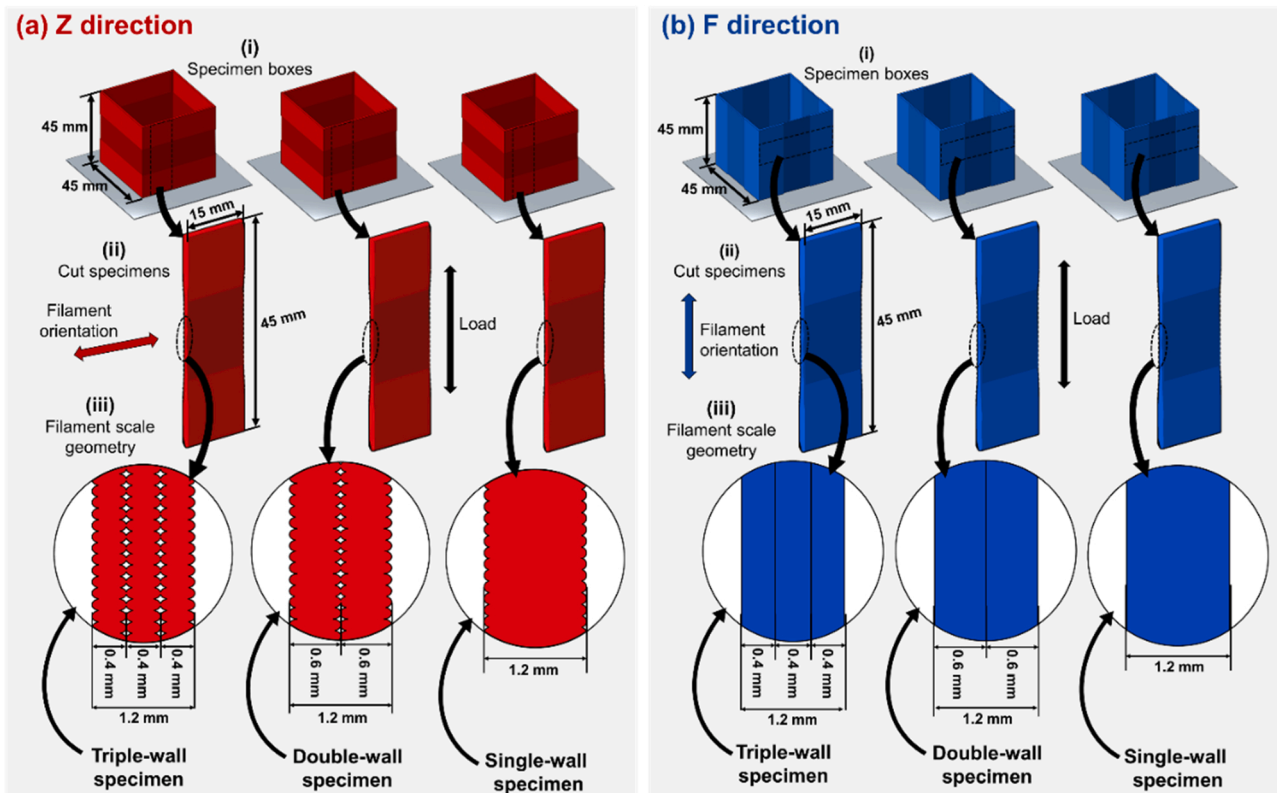


Fig. 1. Manufacture of specimens in Z (a) and F (b) directions. The different specimen geometries were produced as hollow boxes (i) and cut into specimens (ii) with varying cross-sectional geometries: single-wall, double-wall and triple-wall (iii). All specimens had the same overall widths (1.2 mm). The filament orientation, load direction and dimensions are given in (a) and (b).

(a)(i) and (b)(i)) by deposition of:

- a single wall formed by layers of single 1.2 mm-wide extruded filaments;
- a double wall formed by layers of two 0.6 mm-wide extruded filaments;
- a triple wall formed by layers of three 0.4 mm-wide extruded filaments.

Thus, all specimen types had comparable overall width but were formed by using different extruded-filament combinations. To ensure the designed EFWs were achieved, the extrusion rate was adjusted accordingly when generating custom GCode. All specimens were printed at 210 °C with a 60 °C print platform and a constant nozzle print speed of 1000 mm.min<sup>-1</sup>. A 0.4-mm nozzle was utilised to achieve the 0.6 and 0.4 mm EFW (double wall and triple wall) and a 1 mm nozzle was used to achieve the EFW of 1.2 mm (single wall). As demonstrated in previous studies [38,39], it is possible to print extra-wide extrusions (>1 mm) with a 0.4-mm nozzle. However, for the tensile-testing specimen in this study the EFW in grip-sections was 50 % wider than in the gauge section. Therefore, the single-wall specimens required an EFW of 1.8 mm extrusion width and it was not possible to use a 0.4 mm nozzle. All specimens had a layer height of 0.2 mm.

Specimens were produced by deposition of extruded filaments in a symmetrical sequence to achieve hollow four-walled boxes (Fig. 1(a)(i) and (b)(i)). Maintaining a constant speed and direction of the toolpath ensured even heat distribution and cooling gradients across the entire geometry. After manufacturing, the specimen boxes were cut using razor blades, first into single walls and then into specimens with widths of 15 mm (Fig. 1(a)(ii) and (b)(ii)). The respective extruded filament orientations within the specimens and direction of loading are indicated in the images (Fig. 1(a)(ii) and (b)(ii)). Each box yielded eight specimens (two per wall), with five used for mechanical characterisation. The variation in filament-scale geometry and dimensions of each specimen type are illustrated schematically in Fig. 1(a)(iii) and (b)(iii). To achieve the triple-wall structure, each layer was deposited in the prescribed order; the outer wall first, followed by the middle wall, then the internal wall. This was repeated for each subsequent layer. Similarly, in the double-wall structure, the outer wall was printed before the inner wall in each layer.

2.3. Geometrical characterisation

Geometrical characterisation of specimens was undertaken microscopically using a Zeiss Primotech system with 5 × magnification in conjunction with ImageJ software to measure filament-scale features.

2.4. Mechanical characterisation

Specimens were mechanically characterised in uniaxial tension using an Instron 3343 testing system with a 5 kN load cell. The distance between the grips was set at 20 mm. Testing was displacement-controlled with a rate of 0.5 mm.min<sup>-1</sup>. Digital callipers were used to measure the specimen width for calculation of effective strength. Toughness was assessed by measuring the area below the stress-strain plot for each specimen.

2.5. Finite element analysis

To validate the experiment data, FEA was carried out using MSC software. The optical images of the specimens with one, two and three walls (see Section 2.1) were used to obtain the geometric data to develop FE models. Table 1 shows the geometric data employed in each simulation, as well as the number of elements and nodes. The element type was Plane Strain Type19 Quad4, as it accurately replicates non-linear large deformations.

Table 1

The geometrical data, number of elements and nodes used for each simulation.

Parameters	Triple-wall	Double-wall	Single-wall
Width (µm)	1130		1219
Bond (µm)	778	1117	1129
Height (µm)	200	900	200
Notch Radius (µm)	5	5	5
Bond Angle (°)	64.9	88.1	118.9
Elements	32,469	22,042	11,074
Nodes	32,256	21,887	11,195

The simulations were completed using an elastic-perfectly plastic material model, the parameters for which were obtained from the data for F specimens, which represent the bulk material [31]. Each simulation used the maximum-strain failure criterion, where the local strain in any element could not exceed the maximum strain observed in the bulk material, from the material data sheet, since F specimens in study [31] did not all fail. The maximal force achieved in each simulation was used to calculate bond strength, based on the inter-layer bond area between filaments (i.e., smallest load-bearing cross-section). The material properties used are listed in Table 2.

2.6. Statistical analysis

Statistical analysis was undertaken with analysis of variance (ANOVA) and a subsequent t-test using significant levels of p ≤ 0.05.

3. Results and discussion

3.1. Geometrical characterisation

Given the variation in extruded filament geometries between the single-, double- and triple-wall designs, the specimens were first characterised geometrically to understand their microarchitecture.

3.1.1. Microscopic characterisation

To assess the filament-scale geometries of all specimen types they were analysed microscopically. Particular attention was focused on the Z specimens as it was previously identified that the interlayer geometrical features between extruded filaments significantly influenced mechanical anisotropy [31]. To study the deposited geometries, side-view micrographs of Z specimens were taken (Fig. 2) and the EFWs were measured. As demonstrated in Fig. 2, the number and location of voids was distinctly visible. This was, as expected, due to the variation in both the quantity of extruded filaments through their width (X/Y) and their dimensional variation. While the voids and grooves were fairly apparent in both the triple- and double-wall specimens (Fig. 2(a) and (b), respectively), the unconventionally large width of the single-wall apparently resulted in a minimal presence of grooves (Fig. 2(c)). This supports the previous study by the authors [31], which found that interlayer-bond angles were directly influenced by the

Table 2

Material properties in FE models for all three specimen types.

Properties	Value
Elastic Modulus (GPa)	1.2
Poisson's Ratio	0.3
Stress at Yield (MPa)	60
Strain at Yield	0.05
Strain at Failure (Failure Criteria)	0.1

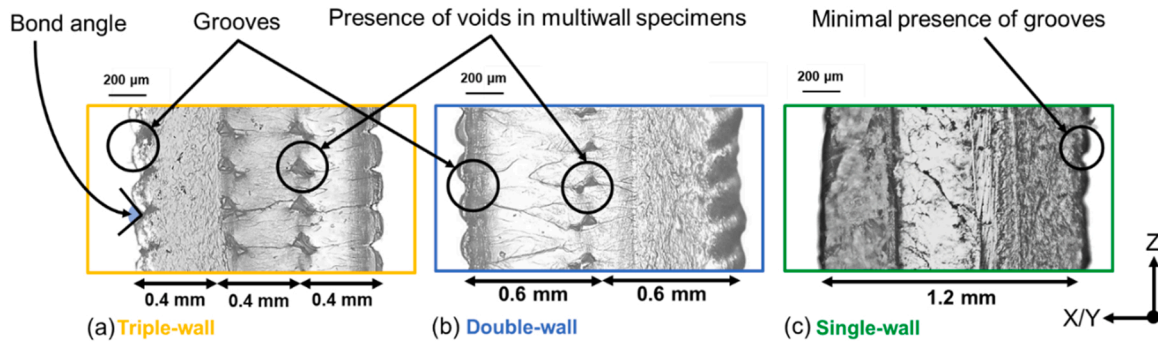


**Fig. 2.** Cross-sectional micrographs of Z specimens with triple-wall (a), double-wall (b) and single-wall (c) structures. Regions of filament-scale geometric features (voids and grooves) are indicated in addition to measurements of EFW in each case.

extruded-filament geometry. Those with higher aspect ratios (EFW to layer height ratio) had less-acute bond angles. Although the volumetric flow rate varied from  $80 \text{ mm}^3 \cdot \text{s}^{-1}$  for triple-wall specimens to  $240 \text{ mm}^3 \cdot \text{s}^{-1}$  for single-wall specimen, the measured widths (recorded in Table 1 as FEA-model input parameters) confirm that the intended flow-rate was achieved and did not exceed the melting capacity of the hot end. The effect of voids and bond angles on mechanical performance is assessed in Sections 3.2.2 and 3.2.3.

**3.1.2. Normalised contact area**

To better understand the influence of the number of extruded filaments in a layer and their dimensions had on the interlayer contact area, the fracture surfaces of Z specimens were analysed (Fig. 3). For each specimen type, the bond width (indicated by the arrow (ii) in (Fig. 3)

and the outer widths (indicated by the arrow (i)) of Z specimens were measured microscopically. In each instance, ten measurements were taken for each wall of the specimen, which yielded a mean outer width and a bond width for each specimen type. The bond width was then normalised by the outer width to provide a normalised contact area. Apparently, the single-wall specimens demonstrated a higher normalised contact area (90 %) (Fig. 3(d)) than the double- and triple-wall ones (76 % and 63 %, respectively). These results indicate that the use of the wide single extruded filament with a large aspect ratio provided a greater interlayer contact area and eliminated interlayer voids, in comparison to the use of multiple smaller extruded filaments with conventional dimensions (0.6 and 0.4 mm). Apparently, the use of two 0.6-mm-wide extruded filaments resulted in a lower void volume than the three 0.4 mm extruded filaments, supporting the trend for improved

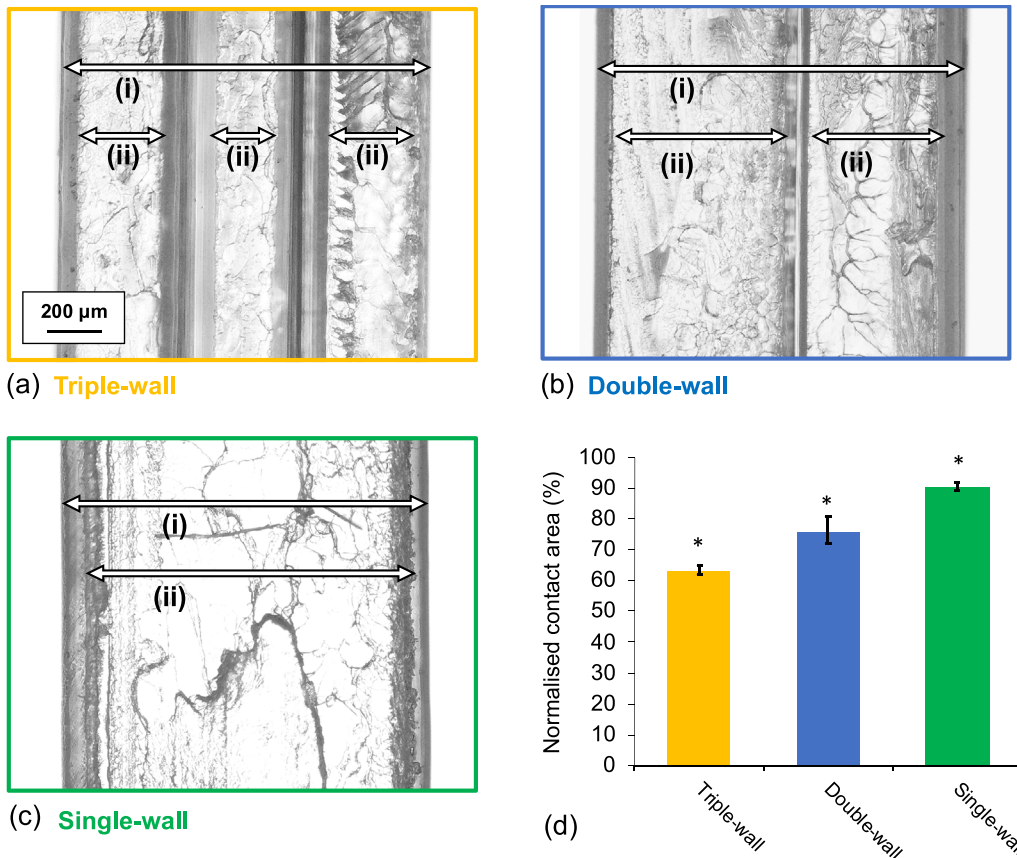


**Fig. 3.** Micrographs showing the overall width (i) and the bonded width (ii) of the triple-wall (a), double-wall (b) and single-wall specimens (c). The normalised contact area (d) was calculated from the measurements of regions (i) and (ii) in (a) to (c). The error bars indicate the range of values for normalised-contact-area measurements for five specimens. \* Indicates significant difference of  $p < 0.05$  between specimen types.

compactness with higher aspect ratios. The mechanical implications of the variation in normalised contact area are considered in Section 3.2.1. This was supported by statistical analysis, which found a significant difference in the contact area between specimen types with different wall geometries ( $p < 0.0001$ ).

### 3.1.3. Bond-angle measurement

The bond angles of each specimen type were measured from the side-view micrographs (Fig. 4). In each instance, 15 measurements were utilised to calculate the mean. For consistency with the single-wall specimens, outer extruded filaments in the double- and triple-wall specimens were used for bond-angle measurement. The results of measurement (Fig. 4) indicated that the deposition of the extra-wide extruded filament achieved a mean bond angle of  $118.9^\circ$ , while the double- and triple-wall specimens demonstrated more acute mean bond angles of  $88.1^\circ$  and  $64.4^\circ$ , respectively. This is explained because wider extrusions (with a greater aspect ratio of EFW divided by LH) required a greater extrusion pressure, which apparently forced the polymer melt to fill voids/grooves more effectively and generate less acute bond angles. This result supports those from the previous study [31], which also demonstrated that increasing the EFW reduced the acuteness of interlayer bonds. In that study, reduction of the bond angle (increased acuteness) was ultimately shown to cause the increased strain concentration. The mechanical effect of the bond angle on the studied structures is analysed in Section 3.2.3. As anticipated, there was a significant difference in the bond angles between the different specimen groups ( $p < 0.0001$ ).

## 3.2. Mechanical characterisation

Given a significant geometrical variation identified for different specimen types, their mechanical analysis is divided into the following sections. Effective strength and stress-strain curves were measured to characterise the strength of the structure with respect to the variation in geometry (Section 3.2.1). Bond strength was measured based on the interlayer contact area of each specimen and analysed both experimentally and through FEA simulations (Section 3.2.2). Strain-at-fracture and toughness were characterised in Section 3.2.3. Geometrical and mechanical anisotropy were assessed by investigating F specimens in

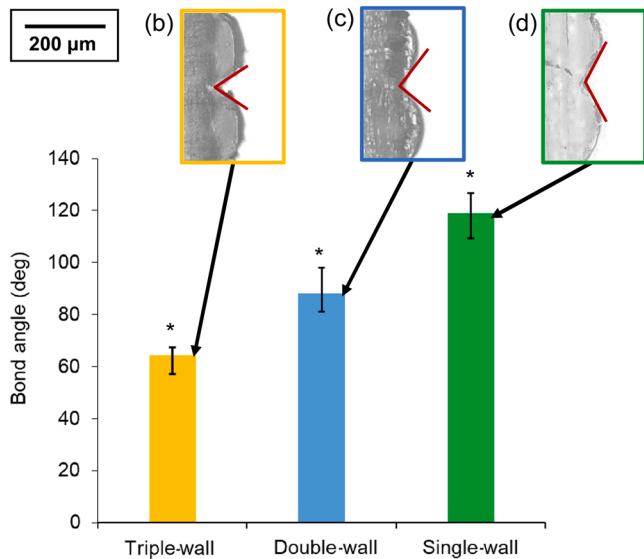


Fig. 4. Mean interlayer bond angles of Z specimens with triple-, double- and single-wall (a), specimens. Error bars indicate the range of values attained for each specimen type from fifteen measurements. Insets (b) to (d) show typical examples of bond-angle measurement for each specimen type. \* Indicates significant difference of  $p < 0.05$  between specimen types.

## Section 3.2.4.

### 3.2.1. Effective strength and stress-strain curves

Effective strength (Fig. 5(a)) was calculated based on width measured with digital callipers, and, thus, this parameter was geometrically dependant on the filament-scale features shown in Sections 3.1.1 and 3.1.2. The single-wall specimen had the greatest effective strength (52.1 MPa), while the double- and triple-wall specimens had reduced mean strengths (39.9 and 37.3 MPa, respectively). Effective stress-strain plots of all specimens illustrate (Fig. 5(b)) that single-wall specimens achieved higher levels of effective stress and strain than the double- and triple-wall specimens. All specimens demonstrated brittle and sudden fracture irrespective of their geometry, typical for the Z direction loading case due to the influence of grooves and bond angles, which caused reduced plasticity and interlayer stress concentration (Section 3.1.3). These findings indicate that the use of extra-wide deposited filaments (1.2 mm) in the single wall specimen provided significant mechanical advantages, resulting in the improved effective strength compared to specimens with conventional multiwall extruded filaments (0.4 and 0.6 mm). The variation in filament-scale geometry caused by changes in the quantity and dimensions of the extruded filaments had a significant influence on their effective strength; specimens with a single extruded filament in the wall demonstrated significantly smaller reductions in mean effective strength compared to the mean bond-strength measurement (only a 10 % reduction) in contrast to significant performance reduction in the double- and triple-wall specimens (by 29 % and

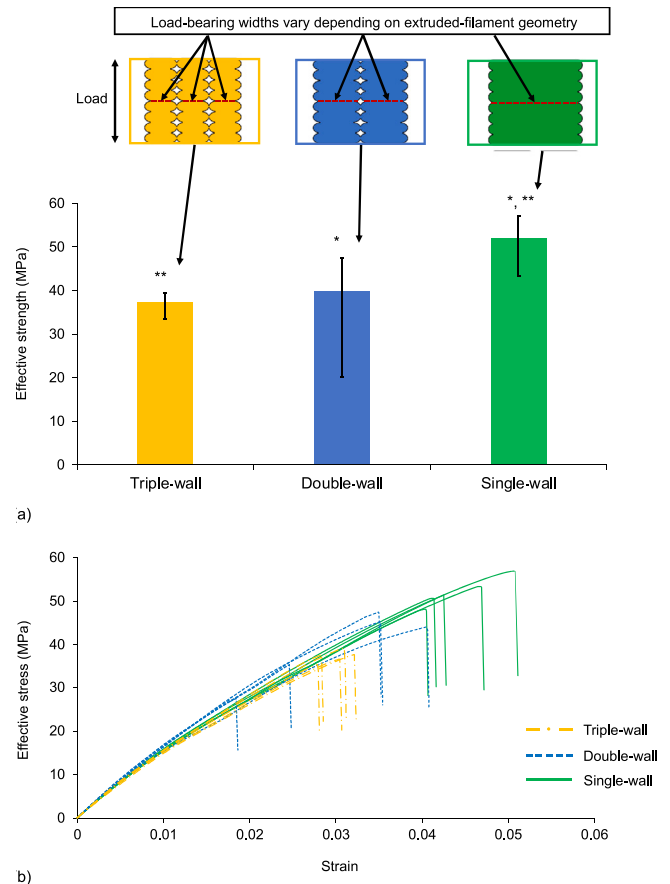


Fig. 5. Mean effective strength (a) and effective stress-strain (b) for Z specimens with triple-, double- and single- wall geometries. Schematic insets in (a) illustrate the variation in load-bearing widths caused by different extruded-filament geometries. The error bars in (a) indicate the range of values attained for five specimens. \* and \*\* indicate significant difference between single-wall with double and trip-wall, respectively.

41 %, respectively) compared to their bond strength. Within the context of the geometrical characterisation (Section 3.1.2), these findings were expected as the normalised contact area of the single-wall specimens was significantly greater (90 %) than that of the double- and triple-wall ones (76 % and 63 %, respectively) (Fig. 3(d)). Apparently, the single-wall specimens provided a more effective distribution of material to bear load, as shown schematically in the insets (Fig. 5(a)). The higher fractions of void area in the double- and triple-wall specimens resulted in the lower contact area in the critical interlayer region, causing the decreasing effective strengths. This was supported by statistical analysis which demonstrated that there was a significant difference between strengths of the single- and double-wall specimens ( $p = 0.0283$ ), similarly, there was a significant difference between the single- and triple-wall specimens ( $p = 0.0003$ ). No significant difference was found between the double- and triple-wall specimens ( $p = 0.5240$ ).

### 3.2.2. Bond strength

When considering only the microscopically measured bond area for strength calculation, all Z specimens were found to have the bulk-material strength irrespective of the quantity or widths of their constituent extruded-filament walls: 63.5, 56.5 and 57.8 MPa for triple-wall, double-wall and single-wall geometries, respectively (Fig. 6). This demonstrated that the variation in the extruded-filament dimensions and the extruded filament quantity did not influence the mechanical performance of the interlayer bonds of the PLA specimens with the mean values of each well within the range of bulk-material properties identified in the literature (Fig. 6). Additionally, these mean bond strengths were attained despite differences in the interlayer cooling times for respective specimen types. Since the printing speed for all specimens was kept constant ( $1000 \text{ mm} \cdot \text{min}^{-1}$ ), each layer of the single wall specimen took approximately 10 s to deposit, while the double and triple walls took approximately 20 and 30 s, respectively. This demonstrated that the bulk-material strength of the interlayer bond in PLA is readily attainable across a range of cooling times, which aligns with the finding of previous studies that bond width is a more important factor than polymer chain entanglement [41], including for a 3-fold change in layer height (and thus extrudate volume) [31], 8-fold change layer time [32] and 16-fold change in printing speed [32]. To achieve changes in layer time, the lengths of the walls of the tensile-testing box were increased. The size of the specimens has also been varied in previous studies, in which widths of 5 mm [30,36] and 15 mm [29,31] had similar properties.

The material used here had no additives to promote interlayer

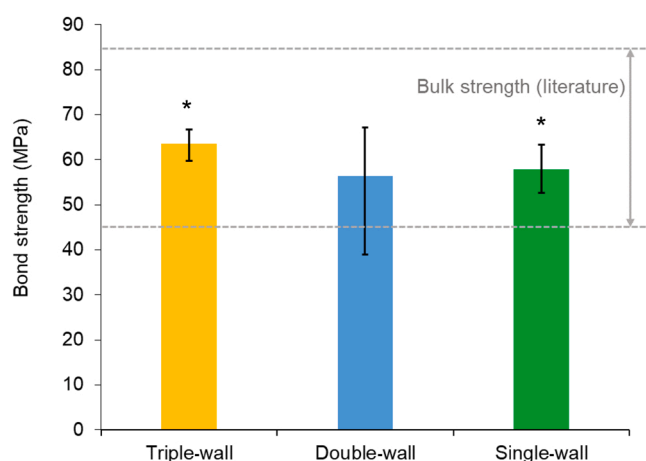


Fig. 6. Mean bond strength of Z specimens with triple-, double- and single-wall geometries. The range of bulk strength values for PLA from the literature [42–49] is included for comparison. Error bars indicate the range of values attained for five specimens. \* Indicates significant difference of  $p < 0.05$  between specimen types.

bonding or similar factors. Although not in scope of this study, the molecular weight distribution of the material has been published previously [36], which considered the molecular weight distribution and degradation of mechanical properties of Z specimens and found no difference between bulk material and Z specimens. Nevertheless, the authors recommend future studies should investigate the effect of extra-wide deposition on mechanical performance of other 3D-printable materials (e.g., polycarbonate, acrylonitrile butadiene styrene and nylon) to confirm the critical importance of bond width relative to polymer chain entanglement.

Given that all specimen types demonstrated close mean bond strengths within the range of bulk strength but differed in terms of their effective strengths, this indicates that the variation in quantity and dimensions of grooves and voids for different specimen types is the distinguishing feature, determining their mechanical performance. Statistical analysis demonstrated that there was no significant difference between the single- and double-wall specimens ( $p = 0.8204$ ) or between the double- and triple-wall specimens ( $p = 0.2676$ ). A statistical difference was found between the single- and triple-wall specimens ( $p = 0.03336$ ), but this is quite close to the statistical threshold ( $p < 0.05$ ) and all specimens had strength values in the range of bulk material identified in the literature [29–32]. Overall, all specimens had bulk strength bond strength, but differences in contact area had the greatest influence on effective strength of the structures (Fig. 5(a)).

The FEA results in Fig. 7 present the distribution of von Mises stress in the Z specimens with triple-, double- and single-wall geometries with their geometries obtained with microscopy for these Z specimen types. The differences in local levels of stress are clearly identifiable by comparing the triple- and single-wall specimens. The line of symmetry for both models coincides with that of one extruded filament, providing a suitable reference for comparison. In the triple-wall specimen, the effective stress varies across two colour bands from the top to the bottom of the repeating unit cell. In contrast, for a similar unit cell in the single-wall specimen, this stress is nearly constant (within the same colour band), indicating behaviour close to that of a solid material without surface geometry and voids. The specific geometry of the filaments (and voids) lead to greater localisation of stresses in the triple-wall specimen, ultimately leading to failure earlier than for a solid material. Similar trends can be found in the vicinity of top/bottom edges of the models. The regions of low stress above/below voids (labelled *region A*) occupy a large part of the specimen's width for higher numbers of filaments. Also, a lower stress occurred in the triple-wall model's top edge than the single-wall model, in both regions A and B, even though the same external strain was applied. The reason for this was more pronounced localisation of stresses (and strains) at the plane of the interface than at the plane half-way up through the height of a filament. This once more highlights the greater variation of stress and strain within the structure with more filaments that can cause failure at lower applied strain. The FEA results demonstrate that non-load-bearing regions in the Z specimens are, in effect, a wasted material (not sustaining loads) still contributing to the weight of the specimens.

The results in Fig. 8(a) demonstrate the comparison between the load data for all three Z specimen types extracted from both FEA simulations and experimental results. The FEA load levels based on the failure criterion were 658 N, 780 N and 956 N for triple-, double- and single-wall geometries, respectively. These data fit well within the range obtained in the experiments (presented by min, max and mean values). Apparently, single-wall specimens provided a more effective spatial distribution of material to bear the load than specimens with increased numbers of filaments through their width. Furthermore, the load data from FEA were used to calculate the bond strength (Fig. 8b) to compare to the experimental results. Again, there was an excellent agreement between the FEA simulations and the experimental results. These findings highlight the importance of the toolpath design to maximise the extrusion width and achieve a more homogenous structure, which is possible without affecting the external part size. Both experimental and

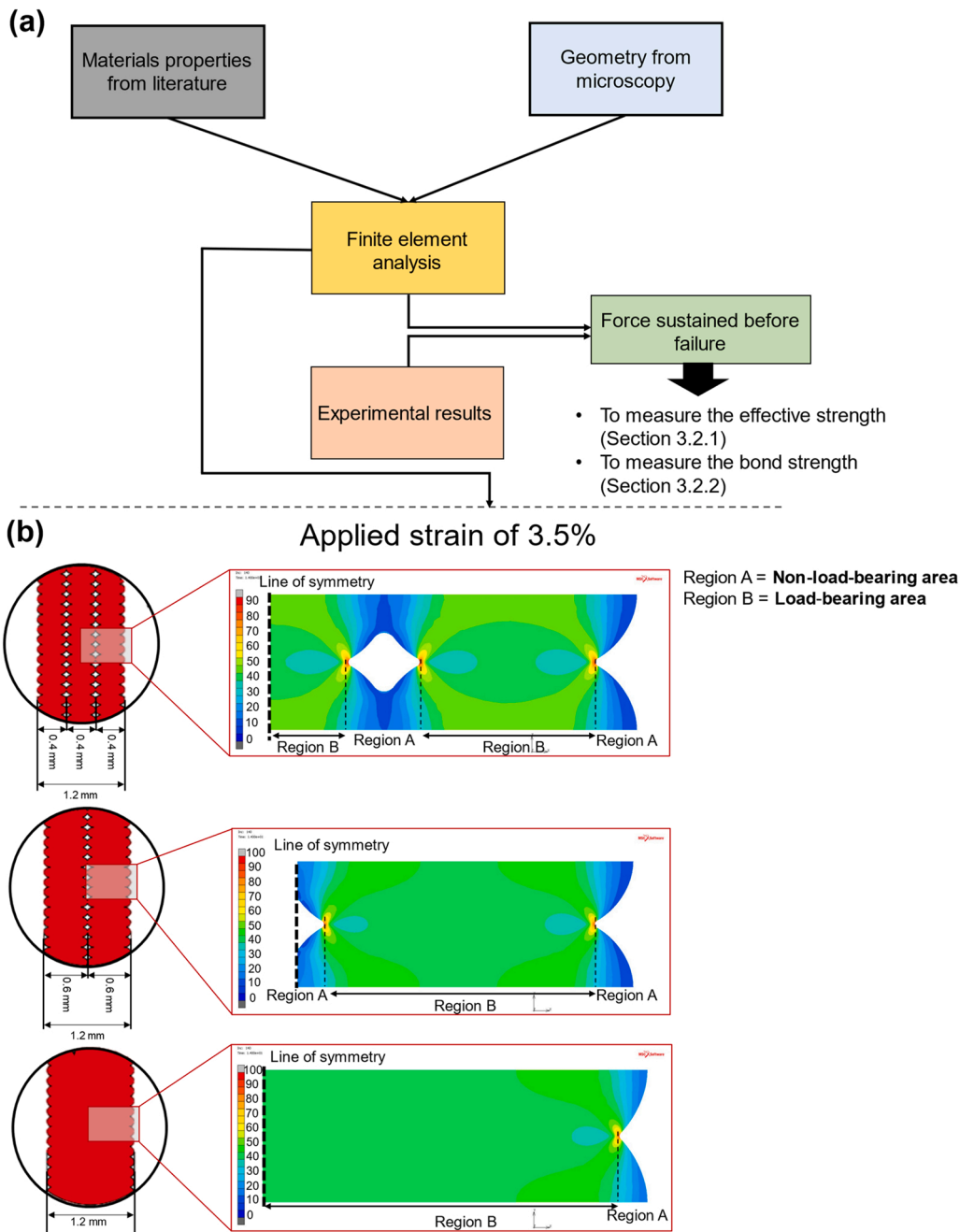


**Fig. 7.** (a) FEA models with materials properties and geometry from microscopy. (b) Distribution of von Misses stress for Z specimens with triple-, double- and single-wall geometries. As the number of EFW increases, the total non-loading-bearing area grows.

simulation studies presented in this study highlighted that since the Z specimens achieved bulk-material strength, existing temperature-based models are not necessary to support analysis of the result. To the authors knowledge, the only study that models bond strength for different extrusion widths [50] found that all specimens printed within the range of print-temperatures recommended by the material manufacturer had interlayer molecular penetration distances of diffusion greater than that required for bulk-material bond strength. Therefore, the strength of those specimens was dependent on the area of the bond between layers. Those findings support the current study results, highlighting the importance of modelling bond area, and indicate that the material used in that study (high impact polystyrene) may be a polymer for which the findings of the present study translate.

The geometry of the extrudates has been demonstrated as being more

important than variation in bond strength between specimen types. This has been reported in a recent review paper [41] which found studies achieved near-isotropic mechanical strength in Z direction for nylon when the specimens had minimal voids. These findings also indicate that the difference in volumetric flow rates between the specimens did not affect interlayer bond strength, and therefore sufficient polymer melting was achieved at all flow rates.

3.2.3. Strain-at-fracture and toughness

The single-wall specimens demonstrated the highest mean strain-at-fracture (0.045) (Fig. 9(a)), 44% and 48% improvements compared to the double – (0.031) and triple-wall (0.030) specimens, respectively. Toughness demonstrated good agreement with the results of strain-at-fracture (Fig. 9(b)); the single-wall specimens attained the highest

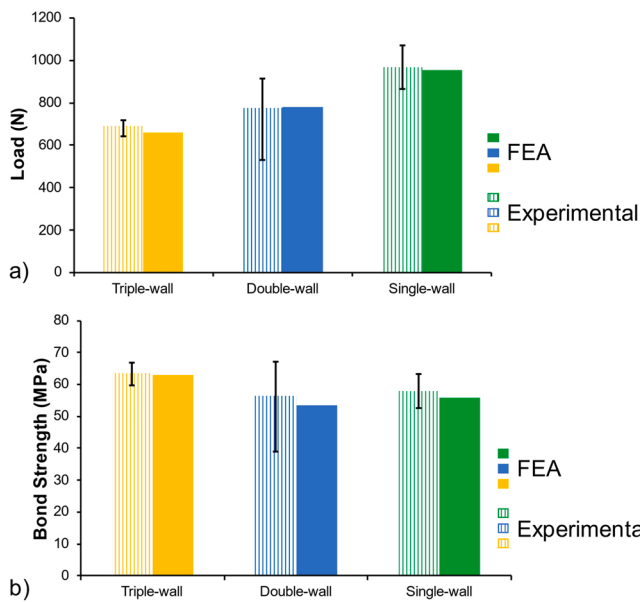


Fig. 8. Maximum load (a) and bond strength (b) obtained from FEA simulations (solid bar) for three Z specimen types compared to experimental values (dashed bar). FEA results support the experimental trends. Error bars indicates the range.

mean toughness ( $1458.3 \text{ kJ.m}^{-3}$ ) compared to the double- and triple-wall ones ( $1033.1$  and  $1066.4 \text{ kJ.m}^{-3}$ , respectively). Thus, improvement for the single-wall specimens was 41 % and 36 % compared to double- and triple-wall ones, respectively. The findings for strain-at-fracture and toughness support those of the previous Section (3.2.1) in demonstrating that the presence of extra-wide deposited filaments in the single-wall specimens enabled greater deformation prior to fracture. This was most likely due to the large area of the interlayer bond (analysed microscopically in Section 3.1.2) and minimal presence of filament-scale voids acting as stress raisers. Conversely, the presence of voids between adjacent filaments in double- and triple-wall specimens might cause their reduced mean strain-at-fracture as the bonds acted independently from each other, and the larger number of voids served to concentrate stresses at the interlayer region. A statistically significant difference was found between single- and double-wall specimens ( $p = 0.0223$ ) and between single- and triple-wall specimens ( $p = 0.0010$ ). For double-wall specimens, relatively large variations in strain-at-fracture and toughness were identified compared to other specimen-types. This is believed to be due to normal experimental error. Two of the double-wall specimens arguably failed earlier than may be

expected when inspecting all fifteen curves in Fig. 5(b). If the two lowest-strength specimens were treated as anomalies, the double-wall specimens would have similar error bars to the other two specimen-types and their effective strength and strain-at-fracture properties would be midway between the single-wall and triple-wall specimen. These two specimens were not treated as anomalies here, and hence, no significant difference was identified between double- and triple-wall specimens ( $p = 0.8532$ ). Statistical variation was anticipated given the broad range of strain-at-fracture values recorded, which is common for interlayer performance in MEAM. Statistical analysis results were similar for toughness.

As discussed with respect to geometry in Section 3.1.1 and evidenced in a previous study [31], the low aspect ratio of filaments in double- and triple-wall specimens (3 and 2, respectively) resulted in acute bond angles. This resulted in more significant stress concentration at their interlayer regions compared to the less acute bond angles in the single-wall specimens, with a larger aspect ratio of 6. This explains the geometrical effect of bond angles on the mechanical variation in strain-at-fracture (Fig. 9(a)), as supported by our previous study [31].

### 3.2.4. Filament direction and geometrical anisotropy

To provide an understanding of the influence of extruded-filament orientation on mechanical performance, specimens of each type were also mechanically tested in the direction of extruded filaments (F direction), with effective strength and strain-at-fracture calculated. The mean effective strengths (Fig. 10(a)) of all specimen types were found to be very close: 71.0, 68.1 and 67.3 MPa for the triple-, double- and single-wall specimens, respectively. The Z specimens had slightly reduced bond strength compared to effective strengths of the F specimens. The mean strain-at-fracture of (Fig. 10(b)) was very similar in all F specimens; 0.073, 0.072 and 0.076 for triple-, double- and single-wall cases, respectively. These results showed different trends from the characterisations of the Z-direction performance (Sections 3.2.2 and 3.2.3), which varied depending on the extruded-filament geometry. This can be explained by the differences in the effect of the filament-scale geometrical features depending on the loading orientations. In the Z specimens, the variation in the interlayer contact areas and bond angles directly affected the mechanical performance due to the orientation of the filament-scale features relative to the loading direction, while in the F specimens, these features had a very limited impact as their orientation did not impinge in this loading direction. Analysing the structural anisotropy by comparing the Z and F specimens in terms of their effective strengths showed that the single-wall specimens had the lowest structural anisotropy, with the Z specimens achieving a mean effective strength in Z direction which was 77.4% that of the mean effective F strength. The double- and triple-wall specimens demonstrated significantly greater structural anisotropy, with their Z effective strengths

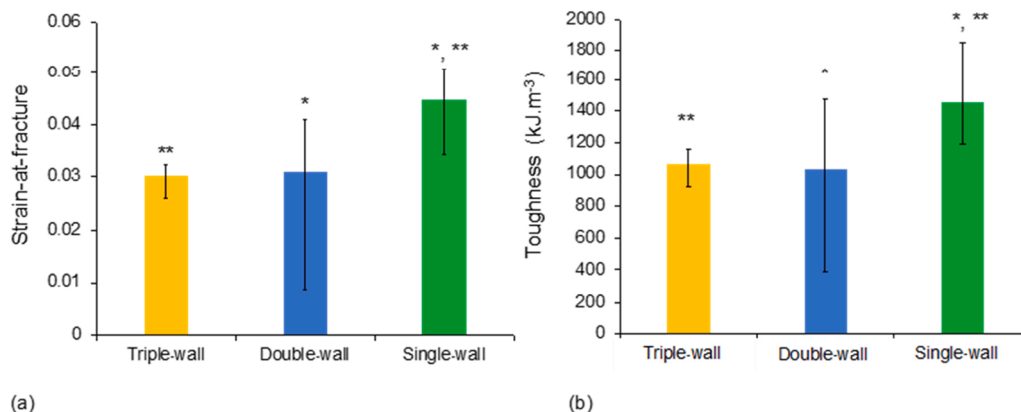
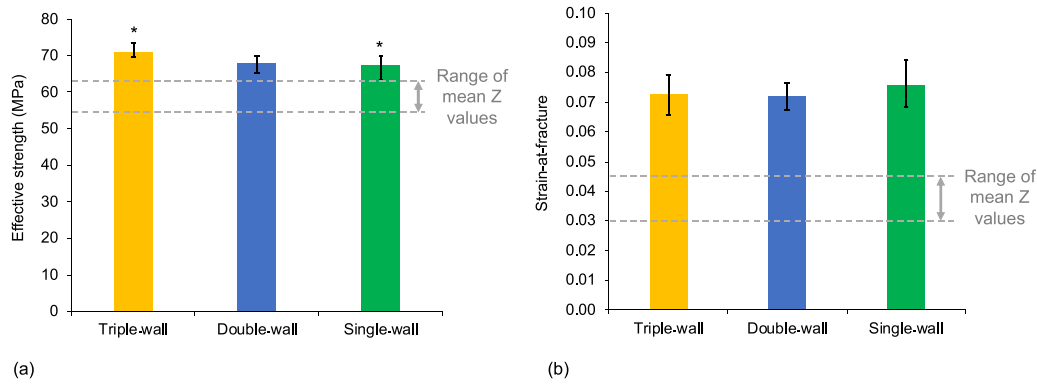


Fig. 9. Mean strain-at-fracture (a) and toughness (b) of Z specimens with single-, double- and triple-wall geometries. Error bars indicate the range of values attained for five specimens \* and \*\* indicate significant difference between single-wall with double and trip-wall, respectively.



**Fig. 10.** Effective strength (a) and strain-at-fracture (b) of F specimens with single-, double- and triple-wall geometry. Error bars indicate the range of results attained for five specimens. \* Indicates significant difference of  $p < 0.05$  between specimen types.

reaching 58.6 % and 52.5 % of that for F direction, respectively. This supports the findings that the geometrical variation of the single-, double- and triple-wall specimens is critical in determining their mechanical performance in the interlayer (Z) direction, with extra-wide extruded filaments showing significant mechanical advantages over the conventional (smaller-width) multi-filament structures. No significant difference was determined between the strength of single- and double-wall specimens ( $p = 0.6091$ ) or between the double- and triple-wall specimens ( $p = 0.0531$ ). A statistical difference was found between the single- and triple-wall specimens ( $p = 0.0210$ ), however, all specimens had strength values in the range of bulk material identified in the literature [29–32]. In terms of strain-at-fracture, no statistical difference was identified between any specimen group.

### 3.3. Application and case studies

The results have broad applicability across the MEAM industry by outlining a methodological convention, which enables significantly improved mechanical performance simply by modifying the geometry of extruded filaments. Given that conventionally, multi-wall schemes are utilised to achieve perimeter structures, the use of extra-wide filament proposed in this study offers not only mechanical but also timesaving benefits. Deposition of a single extra-wide wall showed to be feasible at the same printing speed as small EFWs, thus reducing the printing time by up to 67 % (Fig. 11). The results demonstrated that the use of multi-wall structures with conventional small EFWs caused significant mechanical deficiencies in the Z direction due to filament-scale geometric features at the interlayer bond region. Extra-wide single-filament walls, however, significantly reduced the influence of these factors by suppressing the presence of geometric defects.

Slicing software has the option to set extrusion width. Therefore, the findings here can be implemented in real applications immediately.

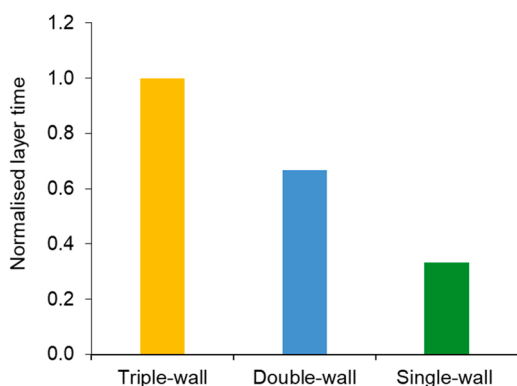


**Fig. 11.** Normalised layer time for single-, double- and triple-wall specimens.

However, there are some limitations of slicing software that mean the use of large extrusion widths may lead to the generation of gaps in the print path. To minimise this issue, options in slicing software to ‘fill gaps’ should be utilised. As an alternative to slicing software, for higher value manufacturing, the print path can be fully defined by writing scripts or using FullControl GCode Designer software [38], which was used in this study.

#### 3.3.1. Industrial case study

The extra-wide extrusion convention was implemented practically through the manufacture of 1000 visors, with support from Toyota Motor Manufacturing UK, for local workers of National Health Service during the Covid-19 pandemic. Designed with the FullControl GCode Designer software [38], visors were printed with nylon filaments with EFW set to 250% of the nozzle diameter. It was possible to reliably print 1-mm-wide extrusions with both 0.4-mm and 0.6-mm nozzles on twenty different printers, providing numerous benefits over the conventional approach, including:

- Improved mechanical integrity, which - through design optimisation - led to a weight reduction of 20 %, diminishing the material consumption.
- A 67 % reduction in the production time meant that up to 3 times more visors could be manufactured in the same timeframe.
- A 67 % reduction in the post-processing time thanks to the reduction of defects during printing.
- Fewer toolpath movements (compared to the multiple narrower extrusions necessary for conventional printing schemes) resulted in improved machine longevity and diminished the maintenance demand.

For the authors of this study, this non-research activity related to design and manufacture of visors highlighted the value of undertaking this research focussed on quantitative data for the opportunities presented by increasing EFW. For high-value or high-throughput parts, extra-wide EFW should be a high-priority consideration when optimising the design and process setup, since it offers the potential for multi-fold benefits in terms of manufacturing time, whilst also potentially increasing mechanical properties by almost 50%. This case study used nylon material, and therefore supports potential translation of the main results of the study (PLA material) to other materials. However, until generality is thoroughly investigated, the extra-wide printing approach should be investigated for each specific material of interest.

#### 3.3.2. 3D-printed lower-limb prosthetic socket

A case study of 3D-printed lower-limb prosthetic socket was also carried out to demonstrate the quality improvement due to the extra-wide deposition compared with standard slicing software. A digital

copy of a transfemoral prosthetic socket of a 14-year-old UK male (74 kg) was used as the build part for demonstration purpose. The cup-like lower-limb prosthetic socket consists of a thin-walled periphery (thickness of 3 mm), where failure occurred in our previous study [51]. Two groups of transfemoral prosthetic sockets (Fig. 12a-b) were manufactured (n = 3 per group) using standard PLA filament on an Ultimaker 2. For one group, the default slicing software was employed, implementing a conventional EFW similar to the nozzle diameter (0.4 mm). Four perimeters were used, which is a relatively high number, since they are known to improve mechanical performance [52]. For another group, the socket was printed with three extra-wide EFWs, each set to 250% of the nozzle diameter. The toolpath was designed with FullControl GCode Designer [38], because the slicer was not able to achieve a neat toolpath with only three filaments. A key area of future research will be to improve slicer algorithms to reliably utilise extra-wide EFWs. All the manufactured prosthetic socket were loaded on an in-house designed socket testing rig (Fig. 12c) according to the ISO10328 standard. The testing condition was based on the maximum load recorded for each test, which should be equivalent to the weight acceptance stage of the gait cycle.

The mean load data are presented in Fig. 12(e). Apparently, the specimens manufactured with the extra-wide deposition convention had significantly improved load-bearing capability ( $p = 0.0001$ ), although they have the same total thickness. Their load bearing capacity exceeded

the maximum load of the testing setup (10 kN) without failing, at which point they already achieved 222% of the load sustained by the specimens with conventional EFW. Such enhanced performance means it would be possible to reduce the thickness of the socket in future designs, which is not possible for the conventional-EFW specimens since they only achieved a mean load 15% above the requirements of ISO10328. Post fracture analysis of the 3D-printed socket (Fig. 12d) revealed a clearly visible delamination for traditional (slicer-based) specimens as opposed to crazing for the specimens with extra-wide EFW. This highlighted the role of interlayer bond strength in these tests, even though the loading scenario was complex, with bending, compression and hoop stresses being more prominent than tension across the interlayer bond. This yield/failure behaviour demonstrated that specimens with conventional EFW were more susceptible to failure due to the presence of voids and gaps as a result of the print path.

Future work should consider the integration of the understanding developed in this study into printing software to enable users to readily achieve these mechanical and time-saving benefits. Since the mechanical benefits of extra-wide extrusions were shown to relate directly with geometrical improvements, further research could consider additional modifications of nozzle geometry to target even larger EFWs. Additionally, development of hardware capable of higher extrusion rates to attain wider extruded filaments could be investigated. From a mechanical perspective, generating more complex structures using extra-

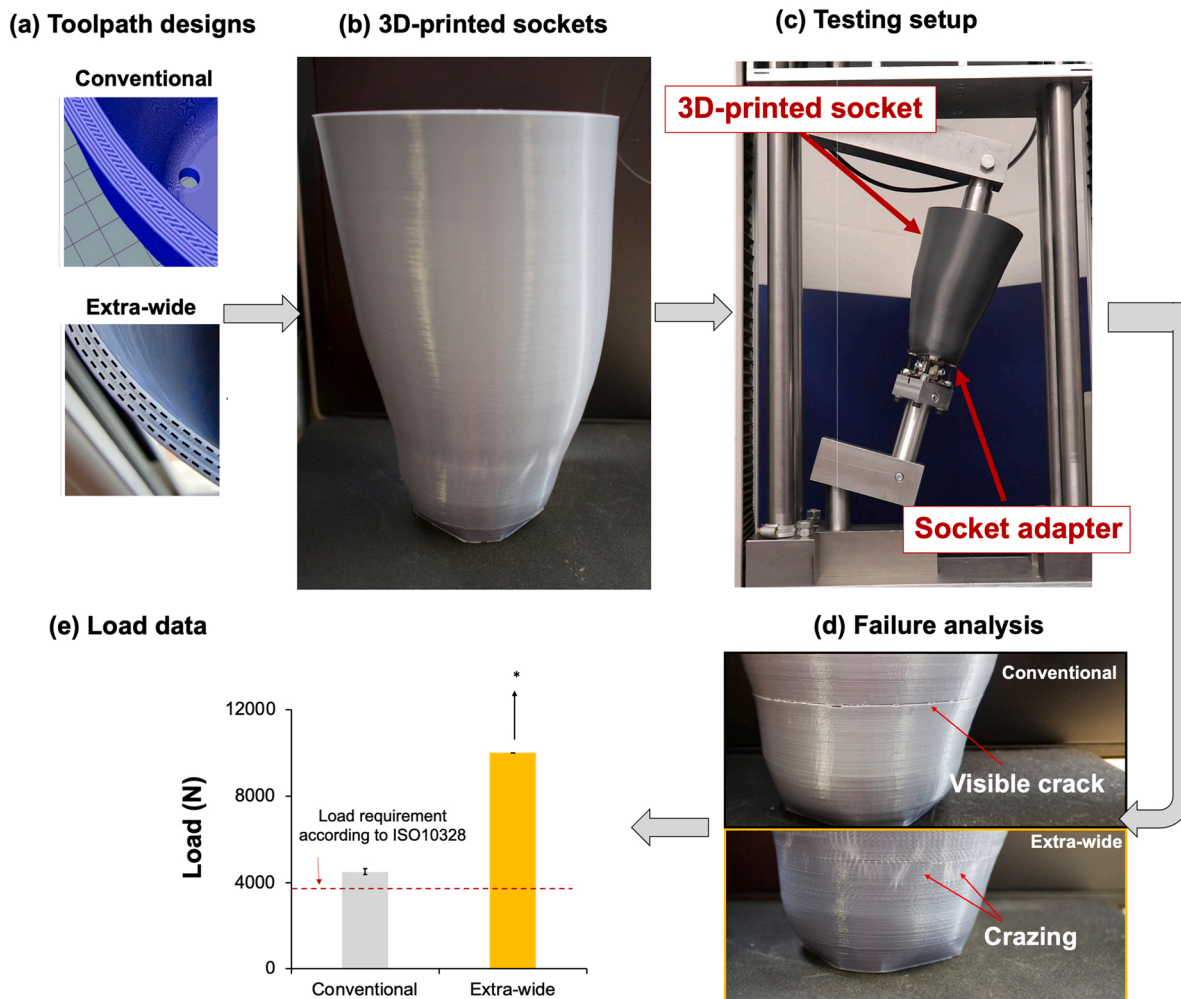


Fig. 12. The case study of the 3D printed socket demonstrating the applicability of the extra-wide deposition convention. (a) Two toolpath designs: using conventional extrusion widths similar to nozzle diameter, and with extra-wide deposition. (b)-(c) Final 3D-printed socket and testing setup. (d) Post-fracture analysis indicating interlayer debonding for conventional specimen and crazing for extra-wide deposition (without failure up to 10 kN). (e) Significantly improved mean load (\*  $p = 0.0001$ ) for extra-wide deposition.

wide extruded filaments and understanding their mechanical properties would be advantageous.

Although the results of this study demonstrated value for PLA, caution must be taken when considering translation to other polymer materials and composites. We believe that the general finding that increasing bond area improves strength will translate to other materials, but future research should check this for specific materials. Results will likely translate best for materials with good interlayer bond strength. In ongoing research for future publication, the authors have found nylon, PLA, high-density polyethylene (HDPE) and polypropylene (PP) to have bond strength similar to the bulk material, whereas ABS, polyethylene terephthalate glycol (PETG) and fibre-filled polymers did not, although the strength was still found to be proportional to the interlayer bond area for those materials. Therefore, the interlayer bond area should be maximised where possible, and the approach described in the present study is one option to consider along with other factors that affect geometry including the overlap percentage between neighbouring filaments, layer height and extrusion temperature. For materials that do not achieve bond strength similar to the bulk material, research should first focus on optimising interlayer bond strength and then attempt to maximise bond area without detrimentally affecting bond strength. In research undertaken for future publication, the authors have successfully printed at 200 % nozzle diameter with several carbon-fibre filled polymers and found good mechanical properties. An interesting area of research for fibre-filled materials would be to determine whether widths > 250% are possible, since it may be expected that fibres impede lateral flow from the nozzle, and how the fibre orientation distribution is affected by wide extrusion.

#### 4. Conclusions

This study demonstrated that using extra-wide extruded filaments (widths of 1.2 mm for a 0.2 mm layer height) provided significant mechanical benefits and considerably reduced structural anisotropy compared with the conventional approach which employs numerous narrow extruded filaments. Strength, strain-at-fracture and toughness were characterised. The use of a single extra-wide extruded filament to replace multiple narrow filaments reduced the presence of filament-scale geometric features and improved the interlayer-contact area between filaments (enabling 90 % interlayer contact relative to the maximum part dimensions). This alleviated the mechanical limitations associated with typical geometrical features caused by acute bond angles and low contact areas (63–76 % for narrower extrusion widths). Characterisation of bond strength demonstrated that perfect bulk-strength interlayer bonding was attained in all studied structure types, highlighting that issues relating to geometry are the fundamental cause of mechanical anisotropy, not interlayer-bond healing, as is frequently reported. Translation of the results of this study (PLA material) to other materials is an important area of future research. The proposed application to replace conventional multi-wall structures with single-wall extra-wide filaments was supported by two case studies, in which the extra-wide extrusion convention was implemented to manufacture 1000 nylon visors and 3D-printed lower limb prosthetic socket, both with extrusion widths set to 250 % of the nozzle diameter. This study demonstrated that utilising extra-wide extrusion enabled improved effective strength (by up to 40 %), strain-at-fracture (by up to 48 %), and toughness (by up to 41 %) while also saving up to 67 % of the printing time for a part with the same overall dimensions. One of the case studies showed even greater influence with an over 100 % improvement in load-bearing capabilities.

#### CRedit authorship contribution statement

**Moetazedian Amirpasha:** Writing – review & editing, Writing – original draft, Methodology, Investigation, Formal analysis, Data curation, Conceptualization. **Gleadall Andrew:** Writing – review & editing,

Writing – original draft, Visualization, Validation, Supervision, Methodology, Investigation, Formal analysis, Data curation, Conceptualization. **Mitchell Niall:** Software, Methodology, Investigation, Data curation. **Marinopoulos Theodoros:** Investigation, Formal analysis, Data curation. **Allum James:** Writing – original draft, Methodology, Investigation, Formal analysis, Data curation, Conceptualization. **McAdam Isaac:** Data curation. **Li Simin:** Supervision, Formal analysis. **Silberschmidt Vadim V:** Writing – review & editing, Visualization, Supervision, Methodology, Formal analysis, Conceptualization.

#### Declaration of Competing interest

The authors declare that they have no known competing financial interests or personal relationships that could have appeared to influence the work reported in this paper.

#### Data availability

Data will be made available on request.

#### Acknowledgements

This research did not receive any specific grant from funding agencies in the public, commercial, or not-for-profit sectors.

#### References

- [1] P. Honigmann, N. Sharma, B. Okolo, U. Popp, B. Msallem, F.M. Thieringer, Patient-specific surgical implants made of 3D printed PEEK: material, technology, and scope of surgical application, *Biomed. Res. Int.* 2018 (2018) 1–8, <https://doi.org/10.1155/2018/4520636>.
- [2] K.C. Wong, 3D-printed patient-specific applications in orthopedics, *Orthop. Res. Rev.* 8 (2016) 57–66, <https://doi.org/10.2147/ORR.S99614>.
- [3] N. Mohan, P. Senthil, S. Vinodh, N. Jayanth, A review on composite materials and process parameters optimisation for the fused deposition modelling process, *Virtual Phys. Prototyp.* 12 (2017) 47–59, <https://doi.org/10.1080/17452759.2016.1274490>.
- [4] P. Mukherjee, K. Cheng, 3D printing and virtual surgical planning in a difficult Bonebridge case, *Virtual Phys. Prototyp.* 14 (2019) 53–58, <https://doi.org/10.1080/17452759.2018.1513797>.
- [5] S. Ravindrababu, Y. Govdeli, Z.W. Wong, E. Kayacan, Evaluation of the influence of build and print orientations of unmanned aerial vehicle parts fabricated using fused deposition modeling process, *J. Manuf. Process.* 34 (2018) 659–666, <https://doi.org/10.1016/j.jmapro.2018.07.007>.
- [6] I.S. Pascariu, S.M. Zaharia, Design and testing of an unmanned aerial vehicle manufactured by fused deposition modeling, *J. Aerosp. Eng.* 33 (2020), 06020002, [https://doi.org/10.1061/\(asce\)as.1943-5525.0001154](https://doi.org/10.1061/(asce)as.1943-5525.0001154).
- [7] D.W. Rosen, A review of synthesis methods for additive manufacturing, *Virtual Phys. Prototyp.* 11 (2016) 305–317, <https://doi.org/10.1080/17452759.2016.1240208>.
- [8] H. Ko, S.K. Moon, K.N. Otto, Design knowledge representation to support personalised additive manufacturing, *Virtual Phys. Prototyp.* 10 (2015) 217–226, <https://doi.org/10.1080/17452759.2015.1107942>.
- [9] D.W. Rosen, Research supporting principles for design for additive manufacturing: this paper provides a comprehensive review on current design principles and strategies for AM, *Virtual Phys. Prototyp.* 9 (2014) 225–232, <https://doi.org/10.1080/17452759.2014.951530>.
- [10] J. Huang, Q. Chen, H. Jiang, B. Zou, L. Li, J. Liu, H. Yu, A survey of design methods for material extrusion polymer 3D printing, *Virtual Phys. Prototyp.* 15 (2020) 148–162, <https://doi.org/10.1080/17452759.2019.1708027>.
- [11] F. Ning, W. Cong, Y. Hu, H. Wang, Additive manufacturing of carbon fiber-reinforced plastic composites using fused deposition modeling: effects of process parameters on tensile properties, *J. Compos. Mater.* 51 (2017) 451–462, <https://doi.org/10.1177/0021998316646169>.
- [12] K.G.J. Christiyen, U. Chandrasekhar, K. Venkateswarlu, A study on the influence of process parameters on the mechanical properties of 3D printed ABS composite, *IOP Conf. Ser. Mater. Sci. Eng.* 114 (2016), 012109, <https://doi.org/10.1088/1757-899X/114/1/012109>.
- [13] A.C. Abbott, G.P. Tandon, R.L. Bradford, H. Koerner, J.W. Baur, Process-structure-property effects on ABS bond strength in fused filament fabrication, *Addit. Manuf.* 19 (2018) 29–38, <https://doi.org/10.1016/j.addma.2017.11.002>.
- [14] A.Q. Pan, Z.F. Huang, R.J. Guo, J. Liu, Effect of FDM process on adhesive strength of polylactic acid (PLA) filament, *Key Eng. Mater.* 667 (2015) 181–186, <https://doi.org/10.4028/www.scientific.net/KEM.667.181>.
- [15] T.J. Coogan, D.O. Kazmer, Bond and part strength in fused deposition modeling, *Rapid Prototyp. J.* 23 (2017) 414–422, <https://doi.org/10.1108/RPJ-03-2016-0050>.

- [16] B.V. Reddy, N.V. Reddy, A. Ghosh, Fused deposition modelling using direct extrusion, *Virtual Phys. Prototyp.* 2 (2007) 51–60, <https://doi.org/10.1080/17452750701336486>.
- [17] N. Aliehdari, J. Christ, R. Tripuraneni, S. Nadimpalli, A. Ameli, Interlayer adhesion and fracture resistance of polymers printed through melt extrusion additive manufacturing process, *Mater. Des.* 156 (2018) 351–361, <https://doi.org/10.1016/j.matdes.2018.07.001>.
- [18] C. Bellehumeur, L. Li, Modeling of bond formation between polymer filaments in the fused deposition modeling process, *J. Manuf. Process.* 6 (2004) 170–178, [https://doi.org/10.1016/S1526-6125\(04\)70071-7](https://doi.org/10.1016/S1526-6125(04)70071-7).
- [19] V.E. Kuznetsov, A.N. Solonin, O.D. Urzhumtsev, R. Schilling, A.G. Tavitov, Strength of PLA components fabricated with fused deposition technology using a desktop 3D printer as a function of geometrical parameters of the process, *Polymers* 10 (2018).
- [20] L. Fang, Y. Yan, O. Agarwal, S. Yao, J.E. Seppala, S.H. Kang, Effects of environmental temperature and humidity on the geometry and strength of polycarbonate specimens prepared by fused filament fabrication, *Materials* 13 (2020) 4414, <https://doi.org/10.3390/ma13194414>.
- [21] S. Guessasma, S. Belhabib, H. Nouri, Microstructure, thermal and mechanical behavior of 3D printed acrylonitrile styrene acrylate, *Macromol. Mater. Eng.* (2019), 1800793, <https://doi.org/10.1002/mame.201800793>.
- [22] A. Bellini, S. Güçeri, Mechanical characterization of parts fabricated using fused deposition modeling, *Rapid Prototyp. J.* 9 (2003) 252–264, <https://doi.org/10.1108/13552540310489631>.
- [23] J. Cantrell, S. Rohde, D. Damiani, R. Gurnani, L. Di Sandro, J. Anton, A. Young, A. Jerez, D. Steinbach, C. Kroese, P. Ifju, Experimental characterization of the mechanical properties of 3D printed ABS and polycarbonate parts, *Conf. Proc. Soc. Exp. Mech. Ser. 3* (2017) 89–105, [https://doi.org/10.1007/978-3-319-41600-7\\_11](https://doi.org/10.1007/978-3-319-41600-7_11).
- [24] M. Faes, E. Ferraris, D. Moens, Influence of inter-layer cooling time on the quasi-static properties of ABS components produced via fused deposition modelling, *Procedia CIRP* 42 (2016) 748–753, <https://doi.org/10.1016/j.procir.2016.02.313>.
- [25] J. Torres, M. Cole, A. Owji, Z. DeMastry, A.P. Gordon, An approach for mechanical property optimization of fused deposition modeling with poly(lactic acid) via design of experiments, *Rapid Prototyp. J.* 22 (2016) 387–404, <https://doi.org/10.1108/RPJ-07-2014-0083>.
- [26] J.A. Travieso-Rodríguez, R. Jerez-Mesa, J. Llumà, O. Traver-Ramos, G. Gomez-Gras, J.J.R. Rovira, Mechanical properties of 3D-printing poly(lactic acid) parts subjected to bending stress and fatigue testing, *Materials* 12 (2019), <https://doi.org/10.3390/ma122333859>.
- [27] M.S. Uddin, M.F.R. Sidek, M.A. Faizal, R. Ghomashchi, A. Pramanik, Evaluating mechanical properties and failure mechanisms of fused deposition modeling acrylonitrile butadiene styrene parts, *J. Manuf. Sci. Eng. Trans. ASME* 139 (2017) 1–12, <https://doi.org/10.1115/1.4036713>.
- [28] S. Ziemian, M. Okwara, C.W. Ziemian, Tensile and fatigue behavior of layered acrylonitrile butadiene styrene, *Rapid Prototyp. J.* 21 (2015) 270–278, <https://doi.org/10.1108/RPJ-09-2013-0086>.
- [29] J. Allum, A. Gleadall, V.V. Silberschmidt, Fracture of 3D-printed polymers: crucial role of filament-scale geometric features, *Eng. Fract. Mech.* 224 (2020), 106818.
- [30] A. Moetazedian, A. Gleadall, X. Han, V.V. Silberschmidt, Effect of environment on mechanical properties of 3D printed polylactide for biomedical applications, *J. Mech. Behav. Biomed. Mater.* 102 (2020), 103510, <https://doi.org/10.1016/j.jmbbm.2019.103510>.
- [31] J. Allum, A. Moetazedian, A. Gleadall, V.V. Silberschmidt, Interlayer bonding has bulk-material strength in extrusion additive manufacturing: new understanding of anisotropy, *Addit. Manuf.* 34 (2020), 101297.
- [32] A. Moetazedian, J. Allum, A. Gleadall, V.V. Silberschmidt, Bulk-material bond strength exists in extrusion additive manufacturing for a wide range of temperatures, speeds, and layer times, *3D Print. Addit. Manuf.* (2021) 1–16, <https://doi.org/10.1089/3dp.2021.0112>.
- [33] J. Allum, A. Gleadall, V.V. Silberschmidt, Fracture of 3D-printed micro-tensile specimens: filament-scale geometry-induced anisotropy, *Procedia Struct. Integr.* 28 (2020) 591–601, <https://doi.org/10.1016/j.prostr.2020.10.069>.
- [34] J. Allum, J. Kitzinger, Y. Li, V.V. Silberschmidt, A. Gleadall, ZigZagZ: Improving mechanical performance in extrusion additive manufacturing by nonplanar toolpaths, *Addit. Manuf.* (2020), <https://doi.org/10.1016/j.addma.2020.101715>.
- [35] P.K. Gurralla, S.P. Regalla, Part strength evolution with bonding between filaments in fused deposition modelling: this paper studies how coalescence of filaments contributes to the strength of final FDM part, *Virtual Phys. Prototyp.* 9 (2014) 141–149, <https://doi.org/10.1080/17452759.2014.913400>.
- [36] A. Moetazedian, A. Gleadall, X. Han, A. Ekinci, E. Mele, V.V. Silberschmidt, Mechanical performance of 3D printed polylactide during degradation, *Addit. Manuf.* 38 (2021), 101764, <https://doi.org/10.1016/j.addma.2020.101764>.
- [37] A. Moetazedian, A. Gleadall, X. Han, V.V. Silberschmidt, Effect of environment on mechanical properties of 3D printed polylactide for biomedical applications, *J. Mech. Behav. Biomed. Mater.* 102 (2020), 103510, <https://doi.org/10.1016/j.jmbbm.2019.103510>.
- [38] A. Gleadall, FullControl GCode Designer: open-source software for unconstrained design in additive manufacturing, *Addit. Manuf.* 46 (2021), 102109.
- [39] A. Moetazedian, A.S. Budisuharto, V.V. Silberschmidt, A. Gleadall, CONVEX (CONtinuously Varied EXtrusion): a new scale of design for additive manufacturing, *Addit. Manuf.* (2020), <https://doi.org/10.1016/j.addma.2020.101576>.
- [40] ASTM International, D1708 – 18: Standard Test Method for Tensile Properties of Plastics By Use of Microtensile, 08, 2018. 1–5. <https://doi.org/10.1520/D1708-18.2>.
- [41] J. Allum, A. Moetazedian, A. Gleadall, V.V. Silberschmidt, Discussion on the microscale geometry as the dominant factor for strength anisotropy in material extrusion additive manufacturing, *Addit. Manuf.* 48 (2021), 102390, <https://doi.org/10.1016/j.addma.2021.102390>.
- [42] W. Song, H. Liu, F. Chen, J. Zhang, Effects of ionomer characteristics on reactions and properties of poly(lactic acid) ternary blends prepared by reactive blending, *Polymers* 53 (2012) 2476–2484.
- [43] C. Zhang, Y. Huang, C. Luo, L. Jiang, Y. Dan, Enhanced ductility of polylactide materials: reactive blending with pre-hot sheared natural rubber, *J. Polym. Res.* 20 (2013) 121–130, <https://doi.org/10.1007/s10965-013-0121-9>.
- [44] H. Zhang, J. Huang, L. Yang, R. Chen, W. Zou, X. Lin, J. Qu, Preparation, characterization and properties of PLA/TiO<sub>2</sub> nanocomposites based on a novel vane extruder, *RSC Adv.* 5 (2015) 4639–4647, <https://doi.org/10.1039/c4ra14538k>.
- [45] T.Y. Qiu, M. Song, L.G. Zhao, Testing, characterization and modelling of mechanical behaviour of poly(lactic acid) and poly(butylene succinate) blends, *Mech. Adv. Mater. Mod. Process.* 2 (2016) 1–11, <https://doi.org/10.1186/s40759-016-0014-9>.
- [46] I. Restrepo, N. Benito, C. Medinam, R.V. Mangalaraja, P. Flores, S. Rodriguez-Llamazares, Development and characterization of poly(vinyl alcohol) stabilized poly(lactic acid)/ZnO nanocomposites, *Mater. Res. Express* 4 (2017), 105019.
- [47] M. Spoerk, F. Arbeiter, H. Cajner, J. Sapkota, C. Holzer, Parametric optimization of intra- and inter-layer strengths in parts produced by extrusion-based additive manufacturing of poly(lactic acid), *J. Appl. Polym. Sci.* 134 (2017) 1–15, <https://doi.org/10.1002/app.45401>.
- [48] Y. Bin, B. Yang, H. Wang, The effect of a small amount of modified microfibrillated cellulose and ethylene-glycidyl methacrylate copolymer on the crystallization behaviors and mechanical properties of polylactic acid, *Polym. Bull.* 75 (2018) 3377–3394, <https://doi.org/10.1007/s00289-017-2215-8>.
- [49] X. Meng, N.A. Nguyen, H. Tekinalp, E. Lara-Curzio, S. Ozcan, Supertough PLA-silane nanohybrids by in situ condensation and grafting, *ACS Sustain. Chem. Eng.* 6 (2018) 1289–1298, <https://doi.org/10.1021/acssuschemeng.7b03650>.
- [50] T.J. Coogan, D.O. Kazmer, Prediction of interlayer strength in material extrusion additive manufacturing, *Addit. Manuf.* 35 (2020), 101368, <https://doi.org/10.1016/j.addma.2020.101368>.
- [51] T. Marinopoulos, S. Li, V.V. Silberschmidt, Structural integrity of 3D-printed prosthetic sockets: an experimental study for paediatric above-knee applications, *Procedia Struct. Integr.* 37 (2021) 139–144, <https://doi.org/10.1016/j.prostr.2022.01.069>.
- [52] C. Lubombo, M. Huneault, Effect of infill patterns on the mechanical performance of lightweight 3D-printed cellular PLA parts, *Mater. Today Commun.* 17 (2018) 214–228.